https://doi.org/10.5194/os-2020-26
Preprint. Discussion started: 2 June 2020

Ocean Science Discussions

The Influence of Turbulent Mixing on the Subsurface Chlorophyll Maximum Layer in the Northern South China Sea

Chenjing Shang[1], Changrong Liang[2, 3], Guiying Chen[2, 3], Yongli Gao[4]

[1]Shenzhen Key Laboratory of Marine Bioresources and Eco-environmental Science, College of Life Science and Oceanography, Shenzhen University, Shenzhen 518060, PR China

[2]State Key Laboratory of Tropical Oceanography, South China Sea Institute of Oceanology, Chinese Academy of Sciences, Guangzhou 510301, China

[3]Southern Marine Science and Engineering Guangdong Laboratory, Guangzhou 511458, China

[4]Equipment Public Service Center, South China Sea Institute of Oceanology, Chinese Academy of Sciences, Guangzhou 510301, China

Correspondence to: Changrong Liang (crliang@scsio.ac.cn)

Abstract. We present observations from deployments of a turbulent microstructure instrument and a CTD package in the northern South China Sea from April to May 2010. From these we determined the turbulent mixing (dissipation rate ε and diapycnal diffusivity κ), nutrients (phosphate, nitrate, and nitrite), nutrient fluxes, and chlorophyll a (Chl-a) in two transects (A and B). Transect A was located in region far away from the Luzon Strait where turbulent mixing in the upper 100 m was weak ($\kappa \sim 10^{-6} - 10^{-4}$ m^2 s^{-1}). Transect B was located in region near the Luzon Strait where the turbulent mixing in the upper 100 m was strong ($\kappa \sim 10^{-5} - 10^{-3}$ m^2 s^{-1}) due to the influence of the internal waves originating from the Luzon strait and the water intrusion from the western Pacific. In both transects, there was a thin subsurface chlorophyll maximum layer (SCML) (0.3-0.7 mg m^{-3}) nested in the water column between ~50 and 100 m. The observations indicate that effects of turbulent mixing on the distributions of nutrient and Chl-a were different in different transects. In transect with weak turbulent mixing, nutrient fluxes induced by turbulent mixing transported nutrients to the SCML but not to the upper water. Nutrients were sufficient to maintain a local SCML

https://doi.org/10.5194/os-2020-26
Preprint. Discussion started: 2 June 2020

phytoplankton population and the SCML remained compact. In transect with strong turbulent mixing, nutrient fluxes induced by turbulent mixing transported nutrients not only to the SCML but also to the upper water, which scatters the nutrients in the water column, and weakens and diffuses the SCML.

1. Introduction

Subsurface chlorophyll maximum layers (SCMLs) are nearly ubiquitous in the ocean, which have significant contribution to the water column biomass and primary production (Cullen, 2015). The depth, thickness, and intensity are the three main factors to characterize the SCML, which are mainly controlled by light attenuation and hydrological dynamic (Gong et al., 2014; G Li et al., 2012; Taguchi, 1980). The hydrological dynamic affecting the SCML includes turbulent mixing, advection, upwelling, mesoscale eddy, and circulation (Hu et al., 2014; Huisman et al., 2006; Kononen et al., 1998; Ledwell et al., 2008; Lu et al., 2010; Vandevelde et al., 1987; Z K Wang and Goodman, 2010; Williams et al., 2013a). Turbulent mixing is ubiquitous in the ocean and varies greatly in time and space. In recent years, more and more studies focused on the influence of turbulent mixing on the nutrient distribution and the nutrient supply of phytoplankton communities (Hales et al., 2009; MacIntyre and Jellison, 2001; Schafstall et al., 2010; Sharples et al., 2007; Tanaka et al., 2012; Tweddle et al., 2013; Williams et al., 2013b). For example, Hales et al. (2009) observed high vertical turbulent nutrient fluxes in the euphotic zone at the New England shelf break front. The averaged nitrate fluxes there were up to 6×10^{-5} mmol N m^{-2} s^{-1}, sufficient to support a net community productivity of 30 mmol C m^{-2} d^{-1}. Schafstall et al. (2010) reported the tidal-induced mixing and diapycnal nutrient fluxes in the Mauritanian upwelling region. Nitrate fluxes at the base of the mixed layer over the continental slope reached a mean value of 12×10^{-2} µmol m^{-2} s^{-1}. Study from

https://doi.org/10.5194/os-2020-26
Preprint. Discussion started: 2 June 2020

Tanaka et al. (2012) revealed that vertical turbulent fluxes sustain the high chlorophyll a (Chl-a) region along the shelf break in the south eastern Bering Sea. Observation from Wang and Goodman (2010) indicated that turbulent mixing modulates the thickness and intensity of SCML in Monterey Bay. These studies indicated that nutrient flux induced by turbulent mixing is an important dynamic factor for redistributing nutrients and supporting primary productivity.

The South China Sea (SCS) is a semi-closed basin characterized by abundant phytoplankton and energetic internal waves. Phytoplankton is dominantly modulated by the nutrient distribution and nutrient supply which are affected by turbulent mixing (Chen, 2005; Chen et al., 2004; Du et al., 2017; Q P Li et al., 2016; Ning et al., 2004; Pan et al., 2012; Ryan et al., 2008; Wong et al., 2007; Yin et al., 2001; Zhang et al., 2016), and the turbulent mixing is commonly related to internal waves (Z Y Liu and Lozovatsky, 2012; Shang et al., 2017; St Laurent, 2008; Tian et al., 2009; Yang et al., 2014). Numbers of internal waves propagate westward form the Luzon Strait into the northern SCS and undergo nonlinear interactions during the propagation, providing a large amount of energy for the turbulent mixing of the SCS (Xie et al., 2018; Zhao and Alford, 2006; Zhao et al., 2004). For example, observation reported by St Laurent (2008) indicated that dissipation rates induced by internal tidal waves in the shelf-break region can be $O(10^{-6})$ W kg^{-1}. Studies from Liu and Lozovatsky (2012) showed that the level of dissipation at the north of 20°N is two times larger than that to the south of 20°N. Measurements conducted by Shang et al. (2017) indicated that the spatial distribution of turbulent mixing in the SCS is uneven. Strong turbulent mixing is mainly limited in the region near the Luzon Strait. The unevenly distributed turbulent mixing might have different effects on the distributions of nutrient and Chl-a in different regions of the SCS. However, few studies have investigated the relationships of the turbulent mixing and distributions of nutrients and

https://doi.org/10.5194/os-2020-26
Preprint. Discussion started: 2 June 2020

Chl-a. Most studies involving nutrient supply and phytoplankton in the SCS focus on upwelling and coastal currents (Gan et al., 2010; Han et al., 2013; Q P Li et al., 2016; K K Liu et al., 2002; J J Wang and Tang, 2014). In this study, the microstructure, Chl-a, and nutrient data obtained from two transects of the northern SCS are used to investigated the impact of turbulent mixing on the distributions of nutrient and Chl-a.

2. Data and method

Physical and biogeochemical measurements were conducted from 26 April to 23 May 2010. Figure 1 shows the stations from which the data we use in this study. These stations are divided into two transects (A and B). Transect A was located in the region far away from the Luzon Strait and transect B was located in the region near the Luzon Strait. Transect A includes six stations (A1-A6) and transect B includes nine stations (B1-B9). Conductivity-temperature-depth (CTD) cast was made at each station to collect hydrological and nutrient data. Temperature and salinity data were documented with the Sea-Bird Electronic 911 plus. Water samples were collected with Niskin bottles from different depths for nutrient extraction. The extraction method has been described by Hu et al. (2014). Sea-water from each depth was pre-filtered through a Whatman GF/F and decanted into a 100 ml polycarbonate bottle, frozen immediately and stored at −20°C prior to analysis in the laboratory. According to the standard colorimetric techniques (Kirkwood et al., 1996), the concentrations of nitrate (NO_3), nitrite (NO_2), and phosphate (PO_4) were analyzed with a flow injection analyzer (Quickchem 8500, Lachat Instruments, USA). Continuous time series of velocity at 5 min intervals and 16 m vertical spacing between 38 and 982 m were obtained from a shipboard acoustic Doppler current profiler (ADCP).

https://doi.org/10.5194/os-2020-26
Preprint. Discussion started: 2 June 2020

Ocean Science
Discussions
Open Access

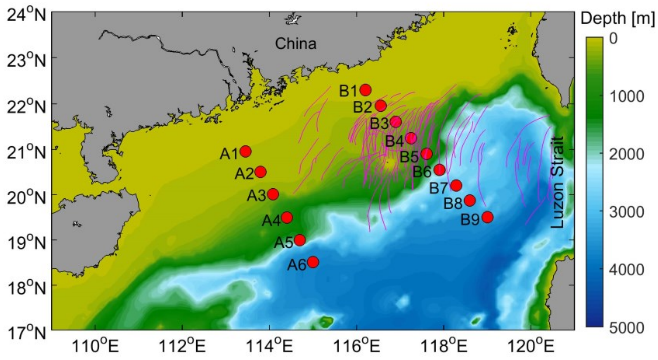

Figure 1: Bottom topography of the northern SCS with stations (circles) shown. Pink curves are internal wave packets derived from satellite images by Zhao et al. (2004).

At all stations except station A4, turbulent microstructure data were collected with the Turbulence Ocean Microstructure Acquisition Profiler (TurboMAP, Rockland Scientific Inc.) (Wolk et al., 2002). TurboMAP is a quasi-free-falling instrument equipped with microstructure shear sensor, temperature sensor, fluorescence sensor, pressure sensor, and turbidity sensor. The parameters collected by TurboMAP include turbulent parameters (microscale velocity shear), bio-optical parameters (fluorescence), and hydrographic parameters (conductivity, temperature, and depth). The sinking rate of the profiler was 0.5-0.7 m s^{-1}. The Chl-a concentration from the fluorescence sensor of TurboMap was calibrated by the bottle sampling. Dissipation rate (ε) was estimated with the observed microscale velocity shear ($\partial u/\partial z$) using the following isotropic formula:

$$\varepsilon = 7.5\nu\left\langle\left(\frac{\partial u}{\partial z}\right)^2\right\rangle = 7.5\nu\int_{k_1}^{k_2}\psi(k)\,dk, \qquad (1)$$

where ν is the kinematic viscosity, < > denotes the spatial average, and $\psi(k)$ is the shear spectrum. k_1 and k_2 are the integration limits. The lower integration limit k_1 is set to 1 cpm and the upper limit k_2 is the highest wavenumber that is not contaminated by vibration noise.

https://doi.org/10.5194/os-2020-26
Preprint. Discussion started: 2 June 2020

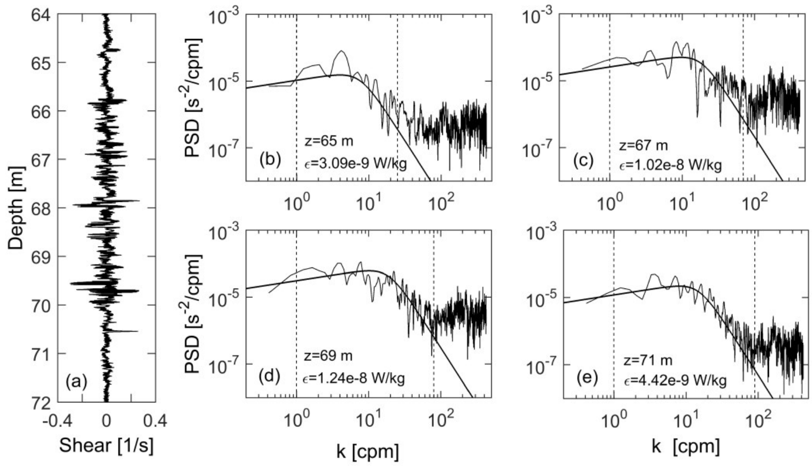

Figure 2: Examples of microscale velocity shear (a) at specified depth segments and the corresponding dissipation spectra (b-e). The smooth curves overlapping on the dissipation spectra are the Nasmyth spectra. The dashed vertical lines indicate the integration limit ranges.

Examples of microscale velocity shear and their corresponding dissipation spectra are shown in Figure 2. The dissipation spectra are approximately consistent with Nasmyth's spectra (Nasmyth, 1970) within the integration range (between the two dashed vertical lines). Distinct peaks associated with high wavenumbers (beyond the upper integration limit) were caused by instrument vibrations. The weak microscale velocity shears at depths of 65 m and 71 m correspond to weak dissipation ($\varepsilon \sim 10^{-9}$ W kg^{-1}) and strong microscale velocity shears at depths of 67 m and 69 m correspond to strong dissipation ($\varepsilon \sim 10^{-8}$ W kg^{-1}). Diapycnal diffusivity (κ) was calculated based on the dissipation rate and stratification (Osborn, 1980):

$$\kappa = \Gamma \frac{\varepsilon}{N^2}, \qquad (2)$$

where Γ=0.2 is the mixing efficiency (Gregg et al., 2018; Oakey, 1982) and N^2 is the squared buoyancy frequency. N^2 was calculated with the obtained temperature and salinity, which has a resolution of 1 m corresponding to the resolution of ε. The shear variance was calculated as

https://doi.org/10.5194/os-2020-26
Preprint. Discussion started: 2 June 2020

$S^2=(\Delta\overline{U}/\Delta z)^2+(\Delta\overline{V}/\Delta z)^2$ with Δz=16 m, where $\overline{U}$ and $\overline{V}$ are the respective zonal and meridional components of the mean horizontal velocity obtained from the shipboard ADCP. The mean velocity is averaged over the time intervals of the TurboMAP measurements.

3. Results

3.1 Hydrographic condition

Intrusion of water from the western Pacific can influence the water properties of the SCS. Measurements and models (Shaw, 1991; Wu and Hsin, 2012) have confirmed that there is a strong intrusion of water from the western Pacific into the SCS through the Luzon Strait. The *T-S* curves of the two transects and the western Pacific are given in Figure 3. Data of the western Pacific (18.5^{o} N-22.5^{o} N, 124.5^{o} E-128.5^{o} E) were obtained from the World Ocean Database 2013. The *T-S* curve of the western Pacific shows a reversed 'S' shape with one salinity minimum and one salinity maximum. The maximum salinity layer (22.5-25.5 kg m^{-3}) corresponds to the high-salinity North Pacific Tropical Water (NPTW) and the minimum salinity layer (25.5-27.5 kg m^{-3}) corresponds to the low-salinity North Pacific Intermediate Water (NPIW) (Qu et al., 2000). NPTW mainly occupies the water column in the upper 200 m and NPIW mainly occupies the water column below. The salinity of transect B was close to the NPTW value in the maximum salinity layer. However, the salinity of transect A was significantly smaller than that of NPTW. These observations indicate that the influence of NPTW intrusion on the water properties of transect B was stronger than that of transect A. Reversed trend was found in the minimum salinity layer. The minimum salinity in the western Pacific is smaller than that in the two transects. Small salinity difference between transects A and B and large salinity difference between the western Pacific and the two transects suggest that the influence of NPIW intrusion on the water properties was weak in both transects.

https://doi.org/10.5194/os-2020-26
Preprint. Discussion started: 2 June 2020

Ocean Science
Discussions
Open Access

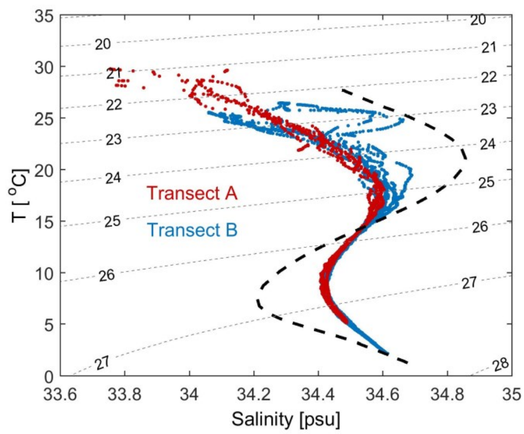

Figure 3: Relation of potential temperature versus salinity with potential density (unit in kg m^{-3}) contours overlaid. The dashed curve shows the relation for potential temperature versus salinity of the western Pacific for reference.

In addition to water intrusion, the SCS is also characterized by energetic internal waves. These waves originate from the Luzon Strait and have strong impact on the velocity and temperature fields of the SCS (Alford et al., 2015). Internal wave packets derived from satellite images by Zhao et al. (2004) are shown in Figure 1 for reference. Transect A was located in the region where few internal waves pass while transect B was located in the region where numbers of internal waves pass. To further investigate the hydrologic condition of these two transects, we show the distributions of temperature and salinity in Figure 4. The temperature in transect A shows a rapid temperature change with increasing depth in the upper 100 m (Figure 4a) while the temperature in transect B remains uniform in the upper 50 m and rapid temperature change mainly occur between 50 and 125 m (Figure 4e). Similar distributions are observed in salinity (Figures 4b and 4f). Rapid salinity change is found in the upper 50 m of transect A while the salinity in the upper 50 m of transect B remains relatively uniform. In the upper 50 m, the temperature of transect A was higher than that of transect

https://doi.org/10.5194/os-2020-26
Preprint. Discussion started: 2 June 2020

B but opposite in the salinity. Water intrusion and internal waves contribute to the difference in hydrological conditions between the two transects. High-salinity NPTW intruded into the SCS through the Luzon Strait and was mixed with the local water of transect B, which results in a high salinity of transect B in the upper layer (Qu et al., 2000). Internal waves might play an important role in mixing the local and invasive waters (Alford et al., 2015).

Using the temperature and salinity data, we estimate the stratification which is showed in Figures 4c and 4g. A comparison of these two transects shows that the surface mixed layer was very thin (<10 m) in transect A but thick (~45 m) in transect B. Below the surface mixed layer is a thermocline with strong stratification. Here, we roughly define the top of the thermocline (that is, the bottom of the surface mixed layer) as the depth at which N^2=1×10^{-4} s^{-2} and the bottom of the thermocline as the depth at which N^2=2×10^{-4} s^{-2}. The thermocline of transect A was mainly limited in the upper 100 m while the thermocline of transect B was found at depth between 45 and 125 m. The thermocline stratification of transect A was stronger than that of transect B. Stratification of transect A between 15 and 35 m reaches 7×10^{-4} s^{-2}. The deep surface mixed layer and weak thermocline stratification of transect B might be caused by the NPTW intrusion and internal waves. Intrusion waters could change the salinity field by mixing with the local waters and internal waves could enhance the turbulent mixing among the waters, which weakens the stratification of transect B. Figures 4d and 4h show the distribution of squared shear for transects A and B, respectively. The squared shear of transect B, evidently, was stronger than that of transect A, especially squared shear at depth of 50-150 m where the level of S^2 was two to three times higher than that of transect A. Strong shear of transect B results from the internal waves originating from Luzon Strait and has important impact on the turbulent mixing.

https://doi.org/10.5194/os-2020-26
Preprint. Discussion started: 2 June 2020

Ocean Science Discussions

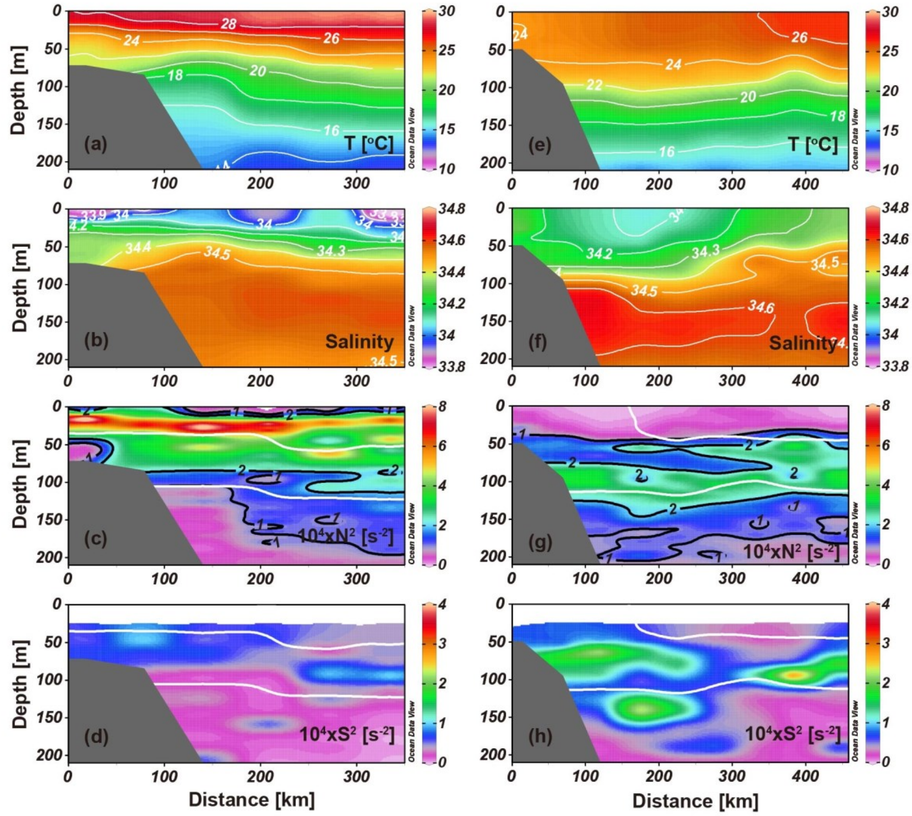

Figure 4: (Left) Distributions of (a) temperature, (b) salinity, (c) squared buoyancy frequency, (d) squared shear for transect A. (Right) The same as (left) but for transect B. Overlaid white lines in (c), (d), (g), and (h) are the boundaries of the subsurface chlorophyll maximum layer. The gray shading indicates the bathymetry.

3.2 Distributions of ε and κ

Transect A has weak shear but strong stratification while transect B has strong shear but weak stratification. Stratification and shear are important conditions for turbulent mixing in the ocean (Liang et al., 2019b; MacKinnon and Gregg, 2003; 2005; Shang et al., 2017). To investigate the effects of stratification and shear on the turbulent mixing, we show the distributions of ε and κ in Figure 5. Data in the upper 10 m was removed due to contamination by the ship's wake and the

https://doi.org/10.5194/os-2020-26
Preprint. Discussion started: 2 June 2020

tilting of the TurboMAP profiler. In both transects, the upper 20 m was occupied by strong dissipations with values of ε reaching $O(10^{-8})$ W kg^{-1} (Figures 5a and 5c). Dissipations of transect B were stronger than that of transect A below 20 m. The averaged ε below 20 m of transect B was 1.92×10^{-8} W kg^{-1}, which is three times larger than that of transect B. Strong dissipations of transect B were mainly caused by internal waves. Energetic internal waves propagate westward from the Luzon Strait to the northern SCS and provide a large amount of energy for dissipation during propagation (Alford et al., 2015; Z Y Liu and Lozovatsky, 2012; Shang et al., 2017). Diapycnal diffusivity shows different distributions in transects A and B (Figures 5b and 5d). Diapycnal diffusivity of transect A has a clear hierarchical structure. A weak diapycnal diffusivity layer with κ of $10^{-7}-10^{-6}$ m^2 s^{-1} occupies the water column between ~20 and 50 m. This weak diapycnal diffusivity layer was mainly due to the strong stratification between ~20 and 50 m (Figure 4c). Strong stratification can suppress shear instability and weaken the diapycnal mixing (Liang et al., 2019b; MacKinnon and Gregg, 2005; Polzin et al., 1996). Below the weak diapycnal diffusivity layer is a slightly enhanced diapycnal diffusivity layer, occupying the water column between ~50 and 100 m. Values of κ in this layer were $10^{-6}-10^{-5}$ m^2 s^{-1}, almost one order of magnitude larger than that of the upper layer. Diapycnal mixing below 100 was weak (κ~ $10^{-7}-10^{-6}$ m^2 s^{-1}). There is no hierarchical structure in the diapycnal mixing of transect B. Strong diapycnal mixing mainly occurred in the upper 100 m and was one to three orders of magnitude larger than that of transect A. The strong turbulent mixing in transect B was related to shear instability of internal waves which depends on the shear and stratification. Generally, Richardson number $Ri=N^2/S^2$ is used to assess the state of a water body and the water body is prone to shear instability in small Richardson number (MacKinnon and Gregg, 2005). Transect A has strong stratification but weak shear (Figures

https://doi.org/10.5194/os-2020-26
Preprint. Discussion started: 2 June 2020

Ocean Science Discussions

4c and 4d) while transect B has weak stratification but strong shear (Figures 4g and 4h), which suggests that the water body in transect B is more prone to shear instability.A roughly estimation of Ri with 16 m shear and stratification indicates that the Ri of transect B is smaller than the Ri of transect A (no shown).

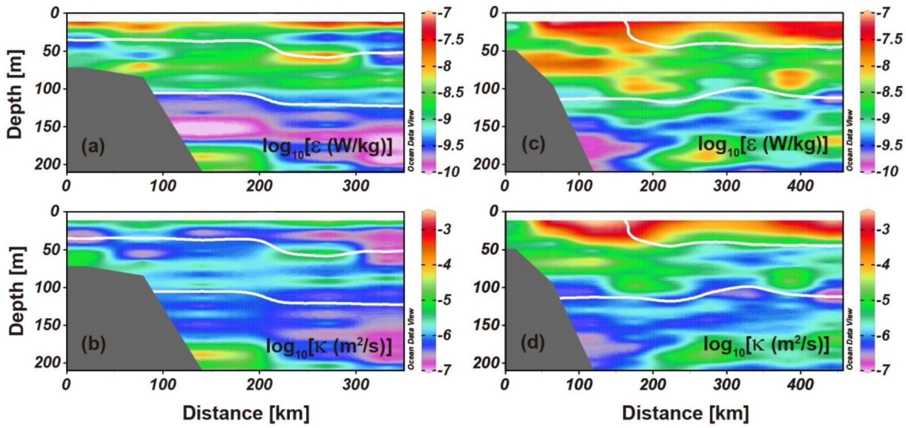

Figure 5: (Left) Distributions of (a) ε and (b) κ for transect A. (Right) The same as (left) but for transect B. Overlaid white lines in each panel are the boundaries of the subsurface chlorophyll maximum layer. The gray shading indicates the bathymetry.

3.3 Distributions of Chl-a and nutrient concentrations

Figures 6a and 6d show the distribution of Chl-a concentration for transects A and B, respectively. The distribution of Chl-a concentration shows a sandwich structure in both transects. A low Chl-a concentration layer with concentration lower than 0.25 mg m^{-3} occupied the upper ~50 m. A high Chl-a concentration layer with concentration higher than 0.25 mg m^{-3} nested in the water column between ~50 and 100 m. This layer is known as subsurface chlorophyll maximum layer. Here we define the boundaries of SCML as the depth at which Chl-a concentration is equal to 0.25 mg m^{-3}. Below the SCML is another low Chl-a concentration layer with concentration lower than

https://doi.org/10.5194/os-2020-26
Preprint. Discussion started: 2 June 2020

0.25 mg m^{-3}. The SCML features of transect A are different from that of transect B. The SCML of transect B occupies the whole water column on continental shelf (0 km<distance<170 km) while transect A retains a hierarchical structure. The maximum Chl-a concentration was relatively stable along transect A, while the maximum Chl-a concentration of transect B decreased at distance of 170-330 km. Overall, the SCML of transect A was more compact than that of transect B.

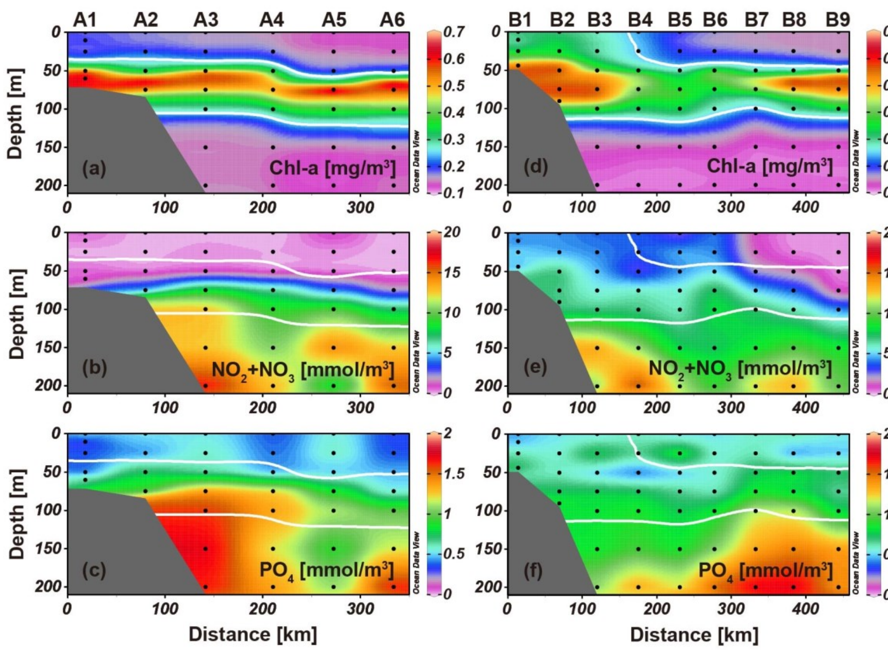

Figure 6: (Left) Distributions of (a) chlorophyll a (chl-a) concentration, (d) nitrate and nitrite (NO_2+NO_3) concentration, (e) phosphate (PO_4) concentration for transect A. (Right) The same as (left) but for transect B. Overlaid white lines in each panel are the boundaries of the subsurface chlorophyll maximum layer. Solid dots indicate depths for nutrient collection. The gray shading indicates the bathymetry.

Figures 6b and 6e show the distribution of nitrate and nitrite (NO_2+NO_3) concentration for transects A and B, respectively. In transect A, NO_2+NO_3 concentration distributes evenly in

https://doi.org/10.5194/os-2020-26
Preprint. Discussion started: 2 June 2020

horizontal direction and has a clear nutricline. The water column in the upper 50 m was occupied by NO_2+NO_3 concentration less than 2.5 mmol m^{-3} and water column below 100 m was occupied by NO_2+NO_3 concentration greater than 12.5 mmol m^{-3}. The water column between 50 and 100 m was a nutricline in which the NO_2+NO_3 concentration increases rapidly with increasing depth, from ~2.5 mmol m^{-3} at 50 m to ~12.5 mmol m^{-3} at 100 m. The nutricline almost coincides with the SCML. A different pattern is found in the distribution of transect B. The distribution of NO_2+NO_3 concentration was scattered and chaotic. No nutricline was found in this transect. The water column in upper 75 m was occupied by NO_2+NO_3 concentration with values smaller than 7.5 mmol m^{-3} and water column below 75 m was occupied by NO_2+NO_3 concentration with values larger than 7.5 mmol m^{-3}. Overall, transect B had more NO_2+NO_3 than transect A above 75 m, but less NO_2+NO_3 than transect A below 75 m. Similarly, transect A also had a clear nutricline between 50 and 100 m in the distribution of PO_4 concentration (Figure 6c) and no nutricline was found in the distribution of PO_4 concentration of transect B (Figure 6f). Transect B had more PO_4 than transect A above 75 m, but less PO_4 than transect A below 75 m.

4. Discussions

Both transects have a high Chl-a concentration layer (SCML) nested in the water column between ~50 and 100 m. However, the SCML of transect A was more compact than that of transect B. In addition, the nutrient distributions (NO_2+NO_3 and PO_4) of transect B were more scattered and chaotic than that of transect A. Turbulent mixing plays an important role in redistributing momentum, heat, nutrients, and microorganisms in the ocean (Inall et al., 2001; Liang et al., 2019a; Shroyer et al., 2010). To investigate the impact of turbulent mixing on the distribution of nutrients, we estimate the nutrient flux induced by turbulent mixing, which is calculated as (Schafstall et al., 2010)

https://doi.org/10.5194/os-2020-26
Preprint. Discussion started: 2 June 2020

Ocean Science Discussions
Open Access

$$\Phi = -\kappa \frac{dC}{dz}, \qquad (3)$$

where dC/dz is the vertical gradient of the dissolved nutrient concentration in the sample. To calculate the nutrient flux, nutrient concentration was first interpolated onto the diapycnal diffusivity grid. For simplicity, we designate the vertical gradient of NO_2+NO_3 concentration as N_z, the vertical gradient of PO_4 concentration as P_z, the NO_2+NO_3 flux as Φ_N, and the PO_4 flux as Φ_P. The distributions of nutrient flux are given in Figures 7a, 7b ,7e, and 7f. Nutrient fluxes in transect A show a multi-layer structure (Figures 7a and 7b). A strong nutrient flux layer occupies the upper 20 m with Φ_N and Φ_P being 10^{-7} mmol m^{-2} s^{-1} and 10^{-8} mmol m^{-2} s^{-1}, respectively. These strong nutrient fluxes mainly resulted from strong turbulent mixing, as evidenced by the observations that values of κ were large (Figure 5b) but values of N_z and P_z were almost zero (Figures 7c and 7d) in the upper 20 m. Lying below the strong nutrient flux layer is a weak nutrient flux layer (Φ_N~10^{-8} mmol m^{-2} s^{-1} and Φ_P~10^{-9} mmol m^{-2} s^{-1}), which occupies the water column between ~20 and 50 m. Weak nutrient fluxes in this layer were mainly due to the small vertical nutrient gradient (Figures 7c and 7d) and weak turbulent mixing (Figure 5b). Most of N_z were smaller than 0.1 mmol m^{-4} (Figure 7c), P_z smaller than 0.01 mmol m^{-4} (Figure 7d), and κ smaller than 5×10^{-7} m^2 s^{-1} (Figure 5b) between ~20 and 50 m. Weak nutrient fluxes indicate that few nutrients were transferred upward from deep layer. Below the weak nutrient flux layer, an enhanced nutrient flux layer (Φ_N~10^{-7} mmol m^{-2} s^{-1} and Φ_P~10^{-8} mmol m^{-2} s^{-1}) exists, occupying the water column between ~50 and 100 m. This layer coincides with the nutricline (Figures 6b and 6c) and the SCML. Both the large vertical nutrient gradient (Figures 7c and 7d) and strong turbulent mixing (Figure 5b) contribute to the strong nutrient fluxes in this layer. Strong nutrient fluxes indicate that nutrients were transferred upward from the deep layer through turbulent mixing. Nutrient fluxes below 100 m were weak due to the small

https://doi.org/10.5194/os-2020-26
Preprint. Discussion started: 2 June 2020

Ocean Science
Discussions
Open Access
EGU

vertical nutrient gradient and weak turbulent mixing.

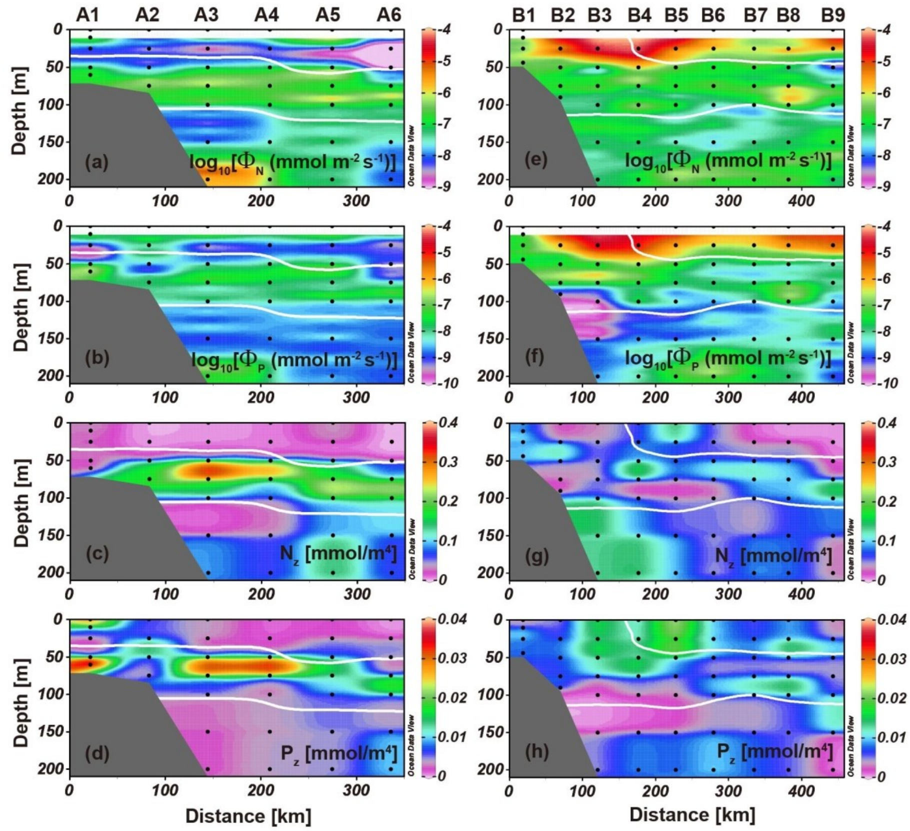

Figure 7: (Left) Distributions of (a) nitrate and nitrite flux (Φ_N), (b) phosphate flux (Φ_P), (c) vertical gradient of nitrate and nitrite concentration (N_z), and (d) vertical gradient of phosphate concentration (P_z) for transect A. (Right) The same as (left) but for transect B. Overlaid white lines in each panel are the boundaries of the subsurface chlorophyll maximum layer. Solid dots are depths for nutrient collection. The gray shading indicates the bathymetry.

A different distribution was found in transect B. The upper 100 m was occupied by strong nutrient fluxes and there was no multi-layer structure (Figures 7e and 7f). Values of Φ_N and Φ_P were one to three orders of magnitude larger than that of transect A. These strong nutrient fluxes were mainly due to strong turbulent mixing, as evidenced by the observations that most values of N_z

https://doi.org/10.5194/os-2020-26
Preprint. Discussion started: 2 June 2020

and P_z were smaller than 0.15 mmol m^{-4} (Figures 7g and 7h) while values of κ can be $O(10^{-4})$ m^2 s^{-1} (Figure 5e). Strong nutrient fluxes indicate that nutrient transport in water column was strong and nutrients were transported upward from the deep layer. It can be seen from Figures 6b, 6c ,6e, and 6f that transect B has more nutrients than transect A in the upper 75 m but fewer nutrients than transect A below 75 m. Strong nutrient fluxes induced by turbulent mixing also made the nutrient distribution of transect B more scattered and chaotic than that of transect A. Next, we analyse the effect of turbulent mixing on the Chl-a distribution.

In transect A, turbulent mixing in the upper 50 m was weak and few nutrients were transported upward by the turbulent mixing. Nutrients was insufficient to maintain the phytoplankton population in the upper 50 m, which exacerbates the deficiency of Chl-a. Note that surface phytoplankton bloom earlier in the season might also cause the lack of nutrients in the surface waters. In the SCML, nutrient fluxes induced by turbulent mixing continuously transport nutrients from deep layer to SCML, which is sufficient to maintain a local SCML phytoplankton population and keep the SCML compact (Figure 6a). Chl-a concentration below the SCML was low though nutrients were abundant. This is mainly due to the lack of light in the deep layer. The effect of turbulent mixing on the Chl-a distribution of transect B is different from that of transect A. On the continental shelf (0 km<distance<170 km), Chl-a and nutrients were distributed throughout the water column, and there is no nutricline (Figures 6d and 6e). Strong turbulent mixing and its induced nutrient fluxes might be important factors for the redistribution of nutrients and Chl-a on the continental shelf. Diapycnal diffusivities in the upper 100 m were $10^{-5}-10^{-3}$ m^2 s^{-1} on the continental shelf, one to two orders of magnitude larger than that of transect A. Strong nutrient fluxes induced by turbulent mixing transport nutrients upward from the bottom, which contributes to maintain the phytoplankton

https://doi.org/10.5194/os-2020-26
Preprint. Discussion started: 2 June 2020

Ocean Science
Discussions
Open Access
EGU

population throughout the water column. Away from the continental shelf (170 km<distance<300 km), SCML was also affected by the strong diapycnal mixing (Figure 6d). The SCML can be distinguished, but it is not as compact as that of transect A. Chl-a within the SCML distribute more evenly and the maximum Chl-a concentration was about two times lower than that of transect A. Evenly distributed Chl-a and low maximum Chl-a concentration might be caused by the strong turbulent mixing. Strong turbulent mixing transports nutrients from SCML to the upper water, dispersing nutrients and reducing nutrient concentrations in the SCML. All these factors affect the SCML phytoplankton population in transect B, which makes the SCML less compact and the maximum Chl-a concentration lower than that of transect A. In deep-sea region (300 km<distance<450 km), few nutrients was found in the surface layer and the nutricline become apparent (Figure 6e). This might be due to the weak turbulent mixing between ~50 and 100 m (Figure 5d). At distance of 300-450 km, diapycnal diffusivity between ~50 and 100 m was comparable to that of transect A and shows a hierarchical structure similar to transect A (Figure 5b). The SCML remains compact and the maximum Chl-a concentration in SCML was comparable to that of transect A.

In addition to turbulent mixing, upwelling is another factor affecting the distributions of chlorophyll and nutrient (Q P Li et al., 2016). Unlike the turbulent mixing, the upwelling transports nutrients upward through advection, $-WdC/dz$, where W is the upwelling velocity. Spatial distributions of curl-driven upwelling velocity and wind stress are shown in Figure 8. Upwelling velocity and wind stress are from 3-day mean METOP-ASCAT data (https://coastwatch.pfeg.noaa.gov/erddap/index.html). During the observation of transect A, the wind direction was generally south on the west of the transect and was northeast on the east of the transect. There was strong curl-driven

https://doi.org/10.5194/os-2020-26
Preprint. Discussion started: 2 June 2020

Ocean Science
Discussions

upwelling in this transect and the upwelling at stations A3-A5 can be larger than 10^{-5} m s^{-1}. The wind direction was generally east during the observation of transect B and the velocity field was predominantly dominated by small downwelling. The effects of the strong upwelling on the chlorophyll and nutrient distributions of transect A can be observed in Figures 6a-6c. Both the SCML and nutricline were lifted up by the upwelling and the biggest uplift occurred at station A3-A5 where the upwelling velocity was strongest. Evidence of uplift induced by upwelling was also found in the distributions of temperature and salinity (Figures 4a and 4b). Both isotherm and isohaline were lifted up by upwelling at distance between 100 and 300 km. These observations suggest that the upwelling mainly affect the large scale distribution of nutrients and Chl-a rather than the fine structure. Transect B was predominantly dominated by small downwelling and its effect on the distributions of nutrients and Chl-a was weak. There is no good correlation between the downwelling and the variations of the SCML and nutricline (Figures 6d-6f), which suggests that the scattered distribution of nutrients and Chl-a in transect B is not due to the upwelling or downwelling. The transportation induced by turbulent mixing plays an important role in the scattered distribution of nutrients and Chl-a in transect B.

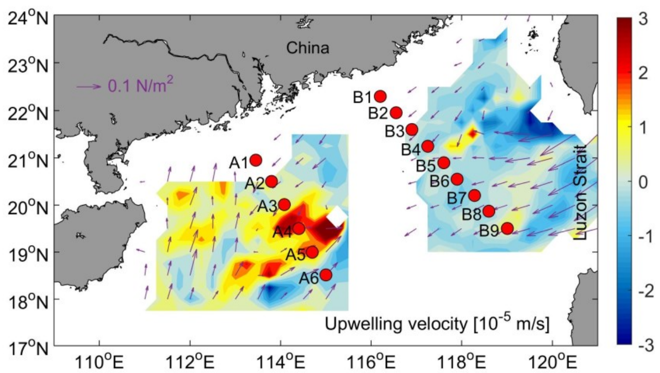

Figure 8: Spatial distributions of curl-driven upwelling velocity (color) and wind stress (vectors)

https://doi.org/10.5194/os-2020-26
Preprint. Discussion started: 2 June 2020

with stations (circles) shown. Upwelling velocity and wind stress are from 3-day mean METOP-ASCAT data.

5. Conclusions

A field experiment has been conducted to study the effects of turbulent mixing on the distributions of nutrients and Chl-a. Two transects were conducted during the experiment (transects A and B). Transect A was located in the region far away from the Luzon Strait and transect B was located in the region near the Luzon Strait where the turbulent mixing is strongly affected by internal waves originating from the Luzon strait and water intrusion from the western Pacific. In both transects, there is a high Chl-a concentration layer (SCML) nested in the water column between ~50 and 100 m. Turbulent mixing plays an important role in transporting nutrients from deep layer to the SCML and maintaining the phytoplankton population. The effects of turbulent mixing on the distributions of nutrients and Chl-a were different in different transects. In transect far away from the Luzon Strait (transect A), the turbulent mixing was relatively weak and nutrients cannot be transported to the surface layer by turbulent mixing. Nutrient fluxes induced by turbulent mixing is sufficient to maintain a local SCML phytoplankton population but insufficient to replenish the surface waters. The SCML remains compact in this transect. In transect near the Luzon Strait (transect B), turbulent mixing was strong due to the influence of internal waves originating from the Luzon strait and water intrusion from the western Pacific. Strong turbulent mixing transports nutrients not only to the SCML but also to the upper waters above the SCML, which disperses nutrient distribution and thus weakens and diffuses the SCML.

Data availability

The research data are available at Zenodo (http://doi.org/10.5281/zenodo.3864885).

https://doi.org/10.5194/os-2020-26
Preprint. Discussion started: 2 June 2020

Author contributions

Chenjing Shang, Guiying Chen, and Yongli Gao designed and carried out the experiments. Changrong Liang prepared the manuscript with contributions from all co-authors.

Competing interests

The authors declare that they have no conflict of interest.

Acknowledgments

This work is supported by the National Key R&D Program of China under contract No. 2018YFA0902500; the National Natural Science Foundation of China under contract Nos 41706137, 41806033 and 41876023; the Natural Science Foundation of Guangdong Province of China under contract No. 2017A030310332; State Key Laboratory of Tropical Oceanography, South China Sea Institute of Oceanology, Chinese Academy of Sciences under contract No. LTO1909; the Natural Science Foundation of SZU under contract Nos 2019078 and 860-000002110258; the Dedicated Fund for Promoting High-Quality Economic Development in Guangdong Province (Marine Economic Development Project) under contract No. GDOE[2019]A03; the Key Special Project for Introduced Talents Team of Southern Marine Science and Engineering Guangdong Laboratory (Guangzhou) under contract No. GML2019ZD0304; the Independent Research Project Program of State Key Laboratory of Tropical Oceanography under contract No. LTOZZ1902. We thank all the crew of the survey ship from the South China Sea Institute of Oceanology, Chinese Academy of Sciences. We are very grateful to Professor Tan Yehui for her advice and nutrient data. The numerical simulation is supported by the High Performance Computing Division and HPC managers of Wei Zhou and Dandan Sui in the South China Sea Institute of Oceanology.

https://doi.org/10.5194/os-2020-26
Preprint. Discussion started: 2 June 2020

References

Alford, M. H., et al.: The formation and fate of internal waves in the South China Sea, *Nature*, *521*(7550), 65-69, doi:10.1038/nature14399, 2015.

Chen, Y. L. L.: Spatial and seasonal variations of nitrate-based new production and primary production in the South China Sea, *Deep-Sea Res Pt I*, *52*(2), 319-340, doi:10.1016/j.dsr.2004.11.001, 2005.

Chen, Y. L. L., H. Y. Chen, D. M. Karl, and M. Takahashi: Nitrogen modulates phytoplankton growth in spring in the South China Sea, *Cont Shelf Res*, *24*(4-5), 527-541, doi:10.1016/j.csr.2003.12.006, 2004.

Cullen, J. J.: Subsurface chlorophyll maximum layers: enduring enigma or mystery solved?, *Annual Review of Marine Science*, *7*, 207-239, 2015.

Du, C. J., Z. Y. Liu, S. J. Kao, and M. H. Dai: Diapycnal Fluxes of Nutrients in an Oligotrophic Oceanic Regime: The South China Sea, *Geophys Res Lett*, *44*(22), 11510-11518, doi:10.1002/2017GL074921, 2017.

Gan, J. P., Z. M. Lu, M. H. Dai, A. Y. Y. Cheung, H. B. Liu, and P. Harrison: Biological response to intensified upwelling and to a river plume in the northeastern South China Sea: A modeling study, *J Geophys Res-Oceans*, *115*, doi:Artn C0900110.1029/2009jc005569, 2010.

Gong, X., J. Shi, and H. Gao: Modeling seasonal variations of subsurface chlorophyll maximum in South China Sea, *J Ocean U China*, *13*(4), 561-571, 2014.

Gregg, M. C., E. A. D'Asaro, J. J. Riley, and E. Kunze: Mixing Efficiency in the Ocean, *Annu Rev Mar Sci*, *10*, 443-473, doi:10.1146/annurev-marine-121916-063643, 2018.

Hales, B., D. Hebert, and J. Marra: Turbulent supply of nutrients to phytoplankton at the New England shelf break front, *J Geophys Res-Oceans*, *114*, doi:10.1029/2008jc005011, 2009.

Han, A. Q., et al.: Inter-shelf nutrient transport from the East China Sea as a major nutrient source supporting winter primary production on the northeast South China Sea shelf, *Biogeosciences*, *10*(12), 8159-8170, doi:10.5194/bg-10-8159-2013, 2013.

Hu, Z. F., Y. H. Tan, X. Y. Song, L. B. Zhou, X. P. Lian, L. M. Huang, and Y. H. He: Influence of mesoscale eddies on primary production in the South China Sea during spring inter-monsoon period, *Acta Oceanol Sin*, *33*(3), 118-128, doi:10.1007/s13131-014-0431-8, 2014.

Huisman, J., N. N. P. Thi, D. M. Karl, and B. Sommeijer: Reduced mixing generates oscillations and chaos in the oceanic deep chlorophyll maximum, *Nature*, *439*(7074), 322, 2006.

Inall, M. E., G. I. Shapiro, and T. J. Sherwin: Mass transport by non-linear internal waves on the Malin Shelf, *Cont*

https://doi.org/10.5194/os-2020-26
Preprint. Discussion started: 2 June 2020

Ocean Science
Discussions

Shelf Res, *21*(13-14), 1449-1472, doi:10.1016/S0278-4343(01)00020-6, 2001.

Kirkwood, D., A. Aminot, and S. Carlberg: The 1994 quasimeme laboratory performance study: Nutrients in seawater and standard solutions, *Mar Pollut Bull*, *32*(8-9), 640-645, 1996.

Kononen, K., S. Hällfors, M. Kokkonen, H. Kuosa, J. Laanemets, J. Pavelson, and R. Autio: Development of a subsurface chlorophyll maximum at the entrance to the Gulf of Finland, Baltic Sea, *Limnol Oceanogr*, *43*(6), 1089-1106, 1998.

Ledwell, J. R., D. J. McGillicuddy Jr, and L. A. Anderson: Nutrient flux into an intense deep chlorophyll layer in a mode-water eddy, *Deep Sea Research Part II: Topical Studies in Oceanography*, *55*(10-13), 1139-1160, 2008.

Li, G., Q. Lin, G. Y. Ni, P. P. Shen, Y. Z. Fan, L. M. Huang, and Y. H. Tan: Vertical patterns of early summer chlorophyll a concentration in the Indian Ocean with special reference to the variation of deep chlorophyll maximum, *Journal of Marine Biology*, *2012*, 2012.

Li, Q. P., Y. Dong, and Y. Wang: Phytoplankton dynamics driven by vertical nutrient fluxes during the spring inter-monsoon period in the northeastern South China Sea, *Biogeosciences*, *13*(2), 455-466, doi:10.5194/bg-13-455-2016, 2016.

Liang, C. R., X. D. Shang, and G. Y. Chen: The vertical heat transport of internal solitary waves over the continental slope in the northern South China Sea, *Acta Oceanol Sin*, *38*(3), 36-44, 2019a.

Liang, C. R., X. D. Shang, Y. F. Qi, G. Y. Chen, and L. H. Yu: Enhanced Diapycnal Mixing Between Water Masses in the Western Equatorial Pacific, *J Geophys Res-Oceans*, *124*(11), 8102-8115, doi:10.1029/2019JC015463, 2019b.

Liu, K. K., S. Y. Chao, P. T. Shaw, G. C. Gong, C. C. Chen, and T. Y. Tang: Monsoon-forced chlorophyll distribution and primary production in the South China Sea: observations and a numerical study, *Deep-Sea Res Pt I*, *49*(8), 1387-1412, doi:Pii S0967-0637(02)00035-3
Doi 10.1016/S0967-0637(02)00035-3, 2002.

Liu, Z. Y., and I. Lozovatsky: Upper pycnocline turbulence in the northern South China Sea, *Chinese Sci Bull*, *57*(18), 2302-2306, doi:10.1007/s11434-012-5137-8, 2012.

Lu, Z., J. Gan, M. Dai, and A. Y. Cheung: The influence of coastal upwelling and a river plume on the subsurface chlorophyll maximum over the shelf of the northeastern South China Sea, *J Marine Syst*, *82*(1-2), 35-46, 2010.

MacIntyre, S., and R. Jellison: Nutrient fluxes from upwelling and enhanced turbulence at the top of the pycnocline in Mono Lake, California, *Hydrobiologia*, *466*(1-3), 13-29, doi:10.1023/A:1014563914112, 2001.

MacKinnon, J. A., and M. C. Gregg: Mixing on the late-summer New England shelf - Solibores, shear, and

https://doi.org/10.5194/os-2020-26
Preprint. Discussion started: 2 June 2020

stratification, *J Phys Oceanogr*, *33*(7), 1476-1492, doi:10.1175/1520-0485(2003)033, 2003.

MacKinnon, J. A., and M. C. Gregg: Spring mixing: Turbulence and internal waves during restratification on the New England shelf, *J Phys Oceanogr*, *35*(12), 2425-2443, doi:10.1175/Jpo2821.1, 2005.

Nasmyth, P. W.: Oceanic turbulence, *Retrospective Theses and Dissertations*, 1919-2007, 1970.

Ning, X., F. Chai, H. Xue, Y. Cai, C. Liu, and J. Shi: Physical-biological oceanographic coupling influencing phytoplankton and primary production in the South China Sea, *J Geophys Res-Oceans*, *109*(C10), doi:10.1029/2004jc002365, 2004.

Oakey, N. S.: Determination of the Rate of Dissipation of Turbulent Energy from Simultaneous Temperature and Velocity Shear Microstructure Measurements, *J Phys Oceanogr*, *12*(3), 256-271, doi:10.1175/1520-0485(1982)012, 1982.

Osborn, T. R.: Estimates of the Local Rate of Vertical Diffusion from Dissipation Measurements, *J Phys Oceanogr*, *10*(1), 83-89, doi:10.1175/1520-0485(1980), 1980.

Pan, X. J., G. T. F. Wong, F. K. Shiah, and T. Y. Ho: Enhancement of biological productivity by internal waves: observations in the summertime in the northern South China Sea, *J Oceanogr*, *68*(3), 427-437, doi:10.1007/s10872-012-0107-y, 2012.

Polzin, K. L., N. S. Oakey, J. M. Toole, and R. W. Schmitt: Fine structure and microstructure characteristics across the northwest Atlantic Subtropical Front, *J Geophys Res-Oceans*, *101*(C6), 14111-14121, doi:10.1029/96jc01020, 1996.

Qu, T., H. Mitsudera, and T. Yamagata: Intrusion of the North Pacific waters into the South China Sea, *J Geophys Res-Oceans*, *105*(C3), 6415-6424, doi:10.1029/1999jc900323, 2000.

Ryan, N. J., S. M. Mitrovic, and L. C. Bowling: Temporal and spatial variability in the phytoplankton community of Myall Lakes, Australia, and influences of salinity, *Hydrobiologia*, *608*, 69-86, doi:10.1007/s10750-008-9375-3, 2008.

Schafstall, J., M. Dengler, P. Brandt, and H. Bange: Tidal-induced mixing and diapycnal nutrient fluxes in the Mauritanian upwelling region, *J Geophys Res-Oceans*, *115*, doi:10.1029/2009jc005940, 2010.

Shang, X. D., C. R. Liang, and G. Y. Chen: Spatial distribution of turbulent mixing in the upper ocean of the South China Sea, *Ocean Sci*, *13*(3), 503, 2017.

Sharples, J., et al.: Spring-neap modulation of internal tide mixing and vertical nitrate fluxes at a shelf edge in summer, *Limnol Oceanogr*, *52*(5), 1735-1747, doi:10.4319/lo.2007.52.5.1735, 2007.

Shaw, P. T.: The Seasonal-Variation of the Intrusion of the Philippine Sea-Water into the South China Sea, *J*

Geophys Res-Oceans, *96*(C1), 821-827, doi:10.1029/90jc02367, 1991.

Shroyer, E. L., J. N. Moum, and J. D. Nash: Vertical heat flux and lateral mass transport in nonlinear internal waves, *Geophys Res Lett*, *37*, L08601, doi:10.1029/2010gl042715, 2010.

St Laurent, L.: Turbulent dissipation on the margins of the South China Sea, *Geophys Res Lett*, *35*(23), L23615, doi:10.1029/2008gl035520, 2008.

Taguchi, S.: Phytoplankton Photosynthesis in the Subsurface Chlorophyll-Maximum Layer of the Tropical North Pacific-Ocean, *J Exp Mar Biol Ecol*, *43*(1), 87-98, doi:10.1016/0022-0981(80)90148-3, 1980.

Tanaka, T., I. Yasuda, K. Kuma, and J. Nishioka: Vertical turbulent iron flux sustains the Green Belt along the shelf break in the southeastern Bering Sea, *Geophys Res Lett*, *39*, doi:10.1029/2012gl051164, 2012.

Tian, J. W., Q. X. Yang, and W. Zhao: Enhanced Diapycnal Mixing in the South China Sea, *J Phys Oceanogr*, *39*(12), 3191-3203, doi: 10.1175/2009jpo3899.1, 2009.

Tweddle, J. F., J. Sharples, M. R. Palmer, K. Davidson, and S. McNeill: Enhanced nutrient fluxes at the shelf sea seasonal thermocline caused by stratified flow over a bank, *Prog Oceanogr*, *117*, 37-47, doi:10.1016/j.pocean.2013.06.018, 2013.

Vandevelde, T., L. Legendre, J.-C. Therriault, S. Demers, and A. Bah: Subsurface chlorophyll maximum and hydrodynamics of the water column, *J Mar Res*, *45*(2), 377-396, 1987.

Wang, J. J., and D. L. Tang: Phytoplankton patchiness during spring intermonsoon in western coast of South China Sea, *Deep-Sea Res Pt Ii*, *101*, 120-128, doi:10.1016/j.dsr2.2013.09.020, 2014.

Wang, Z. K., and L. Goodman: The evolution of a thin phytoplankton layer in strong turbulence, *Cont Shelf Res*, *30*(1), 104-118, doi:10.1016/j.csr.2009.08.006, 2010.

Williams, C., J. Sharples, M. Green, C. Mahaffey, and T. Rippeth: The maintenance of the subsurface chlorophyll maximum in the stratified western Irish Sea, *Limnology and Oceanography: Fluids and Environments*, *3*(1), 61-73, 2013a.

Williams, C., J. Sharples, C. Mahaffey, and T. Rippeth: Wind-driven nutrient pulses to the subsurface chlorophyll maximum in seasonally stratified shelf seas, *Geophys Res Lett*, *40*(20), 5467-5472, doi:10.1002/2013GL058171, 2013b.

Wolk, F., H. Yamazaki, L. Seuront, and R. G. Lueck: A new free-fall profiler for measuring biophysical microstructure, *J Atmos Ocean Tech*, *19*(5), 780-793, doi:10.1175/1520-0426(2002)019, 2002.

Wong, G. T. F., C. M. Tseng, L. S. Wen, and S. W. Chung: Nutrient dynamics and N-anomaly at the SEATS station, *Deep-Sea Res Pt Ii*, *54*(14-15), 1528-1545, doi:10.1016/j.dsr2.2007.05.011, 2007.

https://doi.org/10.5194/os-2020-26
Preprint. Discussion started: 2 June 2020

Wu, C. R., and Y. C. Hsin: The forcing mechanism leading to the Kuroshio intrusion into the South China Sea, *J Geophys Res-Oceans*, *117*(C7), 9, doi:10.1029/2012jc007968, 2012.

Xie, X. H., Q. Liu, Z. X. Zhao, X. D. Shang, S. Q. Cai, D. X. Wang, and D. K. Chen: Deep Sea Currents Driven by Breaking Internal Tides on the Continental Slope, *Geophys Res Lett*, *45*(12), 6160-6166, doi:10.1029/2018GL078372, 2018.

Yang, Q. X., J. W. Tian, W. Zhao, X. F. Liang, and L. Zhou: Observations of turbulence on the shelf and slope of northern South China Sea, *Deep-Sea Res Pt I*, *87*, 43-52, doi:10.1016/j.dsr.2014.02.006, 2014.

Yin, K. D., P. Y. Qian, M. C. S. Wu, J. C. Chen, L. M. Huang, X. Y. Song, and W. J. Jian: Shift from P to N limitation of phytoplankton growth across the Pearl River estuarine plume during summer, *Mar Ecol Prog Ser*, *221*, 17-28, doi:10.3354/Meps221017, 2001.

Zhang, W. Z., H. L. Wang, F. Chai, and G. Q. Qiu: Physical drivers of chlorophyll variability in the open South China Sea, *J Geophys Res-Oceans*, *121*(9), 7123-7140, doi:10.1002/2016JC011983, 2016.

Zhao, Z. X., and M. H. Alford: Source and propagation of internal solitary waves in the northeastern South China Sea, *J Geophys Res-Oceans*, *111*(C11), doi:10.1029/2006jc003644, 2006.

Zhao, Z. X., V. Klemas, Q. N. Zheng, and X. H. Yan: Remote sensing evidence for baroclinic tide origin of internal solitary waves in the northeastern South China Sea, *Geophys Res Lett*, *31*(6), L06302, doi:10.1029/2003gl019077, 2004.